

# Dealing with induced fit, conformational selection and secondary poses in molecular dynamics simulations for reliable free energy predictions

Piero Procacci\*

*Dipartimento di Chimica “Ugo Schiff”, Università degli Studi di Firenze, Via della  
Lastruccia 3, 50019 Sesto Fiorentino, Italy*

E-mail: [piero.procacci@unifi.it](mailto:piero.procacci@unifi.it)

## Abstract

In this study we have tested the performance of standard molecular dynamics simulations (MD), replicates of shorter standard MD simulations, and Hamiltonian Replica Exchange (HREM) simulations for the sampling of two macrocyclic hosts for guests delivery, characterized by induced fit (phenyl-based host) and conformation selection (naphthyl-based host), and of the ODR-BRD4(I) drug-receptor system where the ODR ligand can assume two main poses. For the optimization of the HREM simulation, we have proposed an on-the-fly iterative scheme for equalizing the acceptance ratio along the replica progression at constant replica number.

We have found that while short MD replicates are able to sample as effectively as HREM the diverse conformational states in the phenyl-based host and in the ODR-BRD4(I) complex, in the naphthyl-based macrocycle, characterized by long-lived metastable states, HREM is the only viable alternative for a reliable canonical sampling of the rugged conformational landscape. Implications of these results for free energy calculation of binding free energy in drug-receptor systems are highlighted.

# 1 Introduction

Identification of prospective drugs via a computational approach represents a major challenge in drug discovery. More specifically, elimination of false positive produced in high throughput virtual screening campaigns are still one of the key problems in the early stages of drug design.<sup>1</sup> In a hierarchical, funnel-shaped computational pipeline, hits from cost-effective docking or supervised machine learning approaches, before undergoing wet-lab assessment, are often purged of false positives using expensive molecular dynamics (MD) techniques with a full atomistic description of the system.<sup>2-6</sup>

Most of the current MD applications for computing the ligand-receptor binding affinities are based on the so-called alchemical approach,<sup>7</sup> whereby the build-up of ligand-environment interactions is assessed in the two legs of a thermodynamic cycle (the ligand in the bulk and in the bound state) by constructing a series of intermediate connecting alchemical states. The binding free energy between the physical end states in the two legs of the cycle is recovered as a sum of free energy difference between non physical alchemical states using free energy perturbation<sup>8</sup> and the Bennett acceptance ratio<sup>9</sup> or thermodynamic integration.<sup>10</sup> The *absolute* binding free energy can hence essentially be computed as a difference between two solvation free energies, namely that of the ligand in bulk solvent and in the bound state.<sup>11,12</sup> Alchemical techniques can be likewise adapted to evaluate the relative binding free energy between two *congeneric* compounds by gradually transmuting one compound into the other in a series of “chimeric” states in the two legs of the cycle.<sup>3,13</sup>

Despite progresses in the last decade of algorithms, force fields and methods,<sup>14-16</sup> and despite the spectacular growth of computer power recently boosted by the advent of GPU-CPU heterogeneous high performing computing (HPC) architectures, FEP-based alchemical techniques still faces daunting computational challenges, mostly related to the difficulties in achieving a stationary (converged) sampling<sup>3,17,18</sup> in conformationally complex drug receptor systems. In this respect, molecular recognition is widely thought to be driven by two main mechanisms, namely the induced-fit<sup>19</sup> model or the conformational selection paradigm.<sup>20</sup> According to the former, the protein adapts its conformation upon ligand binding, switching from an *apo* (unbound) to an *holo* (bound) form,

while in the latter case, believed to be the cornerstone of the allosteric effect,<sup>21</sup> binding is possible only when the protein is in one particular conformation among several meta-stable states in chemical equilibrium.

Structural differences between the *holo* and the *apo* form in the induced fit can be difficult to address with FEP-based alchemical approaches due to the long time scale typical of these conformational transitions. Binding through conformational selection relies on the identification of the binding meta-stable state of the protein, sluggishly exchanging between several alternative long-lived conformations, a task that can be achieved only resorting to enhanced sampling techniques such as Hamiltonian Replica Exchange<sup>22-24</sup> (HREM).

Recently, in the context of supramolecular chemistry, two paradigmatic macrocyclic receptors have been designed for induced fit<sup>25</sup> and conformational selection<sup>26</sup> ligand selectivity. The first compound is a structurally flexible macrocyclic cage characterized by two distinct rapidly exchanging conformations due to the flipping of the three phenyl sidewalls connected by methylene bridges. The second compound has a cage with four naphthyl sidewalls whose flipping defines several different, slowly interconverting conformations that can be distinguished in NMR spectra. In the present paper, we have performed extensive MD simulations of these peculiar macrocyclic hosts, showing that a converged free energy conformational landscape, in agreement with experimental indications, can only be achieved using HREM simulations. The limited size of the systems allowed us to test on the fly adaptive protocols for optimizing the efficiency of replica exchange.

Convergence of vanilla MD, MD replicates and HREM with solute tempering have been further assessed and compared in a biologically relevant systems, consisting in the complex of a 3-(trifluoromethyl)phenyl]-5-isoxazolamine compound (ORD) with the first bromodomain-containing protein 4 (BRD4). Such peculiar system is characterized by two distinct ligand poses, whose probability ratio is strongly affected by the alchemical state of the ligand.

The crucial importance, revealed in our study, of enhanced sampling when dealing with common molecular recognition mechanisms, such as induced fit and conformational selection or common phenomena such as pose competition in drug-receptor systems, has important implications in the setting up of automated efficient and reliable alchemical protocol for a high-level screening of docking hits for false positive elimination in drug discovery projects.

## 2 Theoretical background

Typically, events such as conformational transitions in proteins or flexible ligands with large torsional barriers around rotatable bonds occurs abruptly, involving significant changes of the relevant collective coordinate (e.g. a dihedral angle) in a *subpicoseconds* time scale. These rapid transitions, triggered by random collision or concerted fluctuations, are nonetheless *rare*, in the sense that few of them can be observed in a *single* molecule or flexible ligand on a time scale from nanoseconds to milliseconds.<sup>27</sup> In many-molecules systems, rare events become frequent when we test their generic probability irrespective of the molecular index.<sup>28</sup> So, while observing a rare event on *some* molecule is common in a thermodynamic system, it is a matter of pure luck if one is monitoring the behavior of one single molecule during a typical MD simulation lasting few tens of ns. Recently, the advent of GPU and the porting of MD algorithms to GPU architectures has boosted the speed of popular MD codes by more than one order of magnitude.<sup>29–31</sup> A typical solvated drug-receptor system in periodic boundary conditions (50K-100K atoms) can now be run for hundreds of ns per day on a high-end heterogeneous high performing computing (HPC) platform. However, in many cases, this time span can be insufficient for obtaining a statistically converged simulations, since we are dealing with a single-molecule system and not with a thermodynamic ensemble. Unconverged runs on single complexes typically plague the final outcome of the prediction using FEP or TI-based alchemical approaches for binding free energy calculations.<sup>32,33</sup> The sampling problem is patently exposed when results are found to critically depend on similar starting conditions so that in general *replicates* of costly alchemical free energy calculations must be often carried to deliver a reliable prediction with a credible confidence interval.<sup>34–38</sup>

Enhanced sampling techniques are often used to overcome these sampling-related issues. HREM is certainly one of the most effective advanced MD methods for simulating systems with rugged conformational landscapes.<sup>22–24,39,40</sup> HREM is generally engineered to be *collective coordinate agnostic*, scaling the full potential energy of the system or a part of it as in the so-called solute tempering scheme.<sup>23,24,40</sup> This is a significant advantage in drug-receptor systems where we do not generally know *a priori* which collective variables are involved in induced fit or regulating allosteric effects.

In a HREM simulation, several MD simulations are run in parallel on  $n$  states or nodes with gradually scaled potential energy, up to a minimum scaling factor  $s_n = s_{\min}$  such that

$$V_k(\mathbf{x}) = s_k V(\mathbf{x}), \quad s_k = 1, s_1, \dots, s_{\min} \quad (1)$$

Exchanges between scaling factors are periodically attempted, with an acceptance probability based on a Metropolis criterion satisfying the detailed balance condition. In so doing, we observe a random diffusion of the scaling factors (or inverse “temperatures”  $s_k\beta$ ) while the HREM simulation proceeds. A *replica* is hence an MD trajectory spanning various Hamiltonian’s with different scaling factors, providing a mechanism for transmitting conformations sampled in states with strongly scaled potential energy to the *target* (unscaled) state with  $s = 1$  with the correct Boltzmann weight. The acceptance probability  $P_{\text{acc}}(k, k')$  for the  $k \leftrightarrow k'$  exchange depends on the overlap of the corresponding potential energy distributions,<sup>23</sup> so that exchanges are normally attempted between *contiguous* replicas. In this case, we use the short-hand notation  $P_{\text{acc}}(k)$  to denote the acceptance probability for the exchange  $k \leftrightarrow k + 1$ .

The needed number of nodes  $n$  in a HREM simulation depends on the total number of degrees of freedom  $N$  involved in the scaling. As the mean potential energy and its variance are extensive functions, the larger is the number of degrees of freedom involved in the scaling, the more states will be necessary for a significant overlap of contiguous distributions with  $n \propto N^{1/2}$ .<sup>28</sup>

In the generalized ensemble (GE) of the HREM simulation, the replica collection spend by construction the same amount of time on each of the  $n$  states/nodes, independently of the  $P_{\text{acc}}(k)$ . However, the tuning of an HREM simulation for optimal sampling efficiency is by no means a trivial task. As shown in Ref.,<sup>41</sup> the exchange attempt frequency (EAF), one of the parameters of an HREM simulation, should be chosen as high as possible (typically 20-30 ps<sup>-1</sup>) provided that the cost of the attempted exchange is small as it happens when we exchange scaling factors rather than configurations. High  $P_{\text{acc}}(k)$  are in principle desirable but they are costly as they involve a large  $n$ . Like in standard Monte Carlo, it is generally believed that an optimal (and balanced)  $P_{\text{acc}}(k)$  in systems with kinetics traps should be in the range 0.2-0.5. Balancing the acceptance probabilities  $P_{\text{acc}}(k)$  may, in general, result in a smoother replica diffusion across the GE and in a shortening

of the round trip times (RTT). On the other hand, as noted in Ref.,<sup>42</sup> well balanced acceptance ratios along the states progression does not guarantee an optimal *flux* in HREM simulation. The upward flux can be measured as

$$f_u(k) = \frac{z_u(k)}{z_u(k) + z_d(k)} \quad (2)$$

where  $z_u(k)$ ,  $z_d(k)$  are the number of visits to state  $k$  by replicas coming from state 1 (the target state) and from state  $n$ , respectively. Due to replica conservation, we have that  $f_d(k) = 1 - f_u(k)$  where  $f_d(k)$  is the downward flux. Ideally, the optimal flux is obtained when  $f_u(k) = 1 - k/n$  and  $f_d(k) = k/n$ , leading to a *linear* flow distribution with constant transition probabilities. In principle, in a HREM simulation we should try to adapt the scaling ladder to reach such a linear regime for the flux. Flow optimization in HREM is prohibitively costly as it requires long adaptive enhanced sampling simulations to estimate to flux, since many visits to the state  $k$  are necessary to get a statistically reliable  $f_u(k)$ . Severely uneven acceptance ratio using standard scaling factors may on the other hand produce bottlenecks in the replica flow compromising the HREM efficiency. We may hence try to optimize our HREM by balancing the  $P_{\text{acc}}(k)$  on the fly. To this end, starting from the traditional scaling protocol,

$$s_k = s_{\min}^{(k-1)/(n-1)}, \quad (3)$$

whereby overlap between contiguous replica is maximized assuming that the system may be described by an ensemble of harmonic oscillators,<sup>23,43</sup> we propose to periodically reset, with a frequency  $\omega \ll EAF$ , the scaling ladder according to the iterative scheme

$$\Delta s_k^{i+1} = \Delta s_k^i + c\sigma_i(P_{\text{acc}}^i(k) - \langle P_{\text{acc}}^i \rangle) \quad (4)$$

where  $\Delta s_k^i = s_k^i - s_{k+1}^i$  are the  $n - 1$  *positive* differences between contiguous scaling factors for the  $n$  states,  $P_{\text{acc}}^i(k)$  is the acceptance probability for the  $k \leftrightarrow k + 1$  exchange at iteration  $i$ ,  $\langle P_{\text{acc}}^i \rangle = \frac{1}{n-1} \sum P_{\text{acc}}^i(k)$  is the mean acceptance probability at iteration  $i$  and  $\sigma_i$  is the corresponding standard deviation. For an optimal balance of the  $P_{\text{acc}}$ , the final value of  $\sigma_i$  should be as small as possible. According to Eq. 4, the differences  $\Delta s_k^{i+1}$  are corrected by a factor that is strictly

proportional to the product of the standard deviation  $\sigma_i$  and difference between the actual value of  $P_{\text{acc}}(k)^i$  and the mean acceptance ratio. As the sum of the differences,  $\sum_k^{n-1} \Delta s_k^i = 1 - s_{\text{min}}$ , is invariant due to the fact that at each iteration

$$\sum_k^{n-1} \sigma_i (P_{\text{acc}}^i(k) - \langle P_{\text{acc}}^i \rangle) = 0, \quad (5)$$

the update scheme of Eq. 4 is designed to constantly reducing the variance  $\sigma_i^2$  thereby gradually balancing the acceptance probabilities  $P_{\text{acc}}(k)$ . The  $c$  constant, along with the frequency of the scaling reset, regulates the speed of the balancing of the probabilities  $P_{\text{acc}}(k)$ . The probabilities  $P_{\text{acc}}^i(k)$  can be evaluated each few hundreds of attempted exchanges, and hence, with EAF's of the order of 20-30 ps<sup>-1</sup>, a good balancing may be obtained in few ns or less with  $1 < c < 2$  and  $0.001 \times \text{EAF} < \omega < 0.01 \times \text{EAF}$ .

As stated in Ref.,<sup>42</sup> one should be aware of the fact that in complex systems long term transition probabilities are usually different from observed acceptance rates, that are affected by short-time properties. Balancing the acceptance ratio, while avoiding bottlenecks in the replica diffusion, may not necessarily lead to flux linearization.

## 3 Methods

### 3.1 Compounds

In Figure 1, we show the structures of the macrocycles **1** and **2** and of the ligand ODR of the first bromodomain of human BRD4. The structures of **1** and **2** were obtained from Cambridge Crystallographic Data Centre, CCDC 2051483<sup>25</sup> and CCDC 1950443.<sup>26</sup> The phenyl[5]-cage **1** is characterized by two rapidly exchanging structures due to the flipping of the three phenyl side-walls.<sup>25</sup> The two conformation can be distinguished in NMR experiments when **1** selectively binds to quarternary ammonium ions via an induced fit mechanism. Compound **2** (Amide naphatotube) has five different conformations due to the flipping of the non equivalent naphtyl moieties around the amide and aminomethyl junctions. These five conformations are reported in Fig. 2e of Ref.<sup>26</sup> Experimentally, only two (out of five) conformations of the *apo* form of amide naphatotube in apolar

solvents can be distinguished from NMR experiments, indicating that in **2** the exchange occurs in a time scale that exceeds that of NMR (ns to ms). The structures represented in Fig. 1, taken from the Cambridge Structural Database, correspond to the most symmetric ones for compounds **1** and **2**.

Compound ODR is known to be a moderate binder of the BRD4(I) protein with an affinity of  $4.8 \mu\text{M}$ <sup>44</sup>. The initial structure of the complex was obtained from the 3svg PDB file.

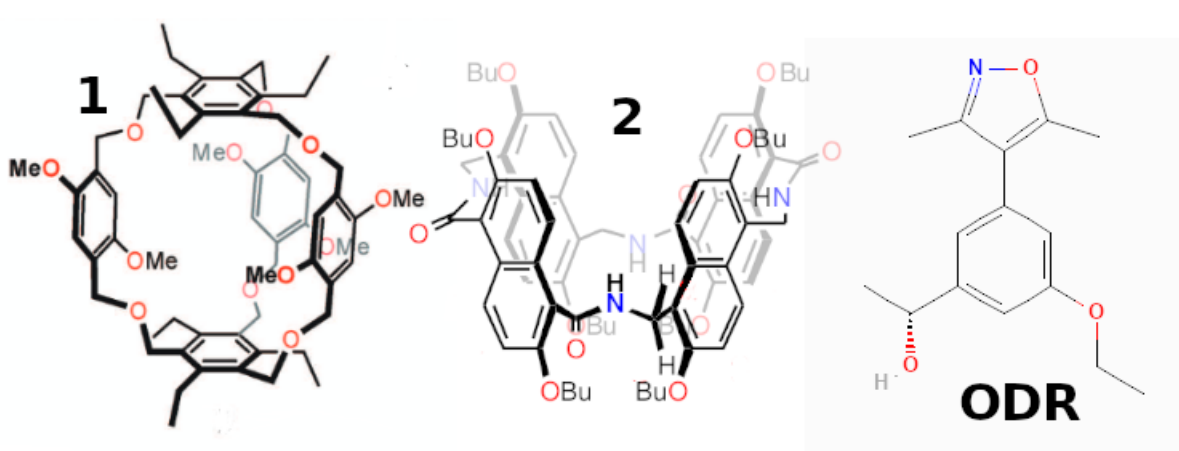


Figure 1: Macrocycles **1** and **2** and the BRD4 ligand ODR

We used the GAFF2 force field for the two macrocycles and the ligand ODR. Assignment and AM1-BCC<sup>45</sup> charge calculations were done using the PrimaDORAC web interface.<sup>46</sup> The BRD4 protein was modeled using the AMBER99SB-ildn force field.<sup>47</sup>

### 3.2 Simulation details

Compound **1** and **2** were simulated *in vacuo*. This was done to sample the full attainable conformational space without mediation of intercalated apolar solvent molecules (such as  $\text{CHCl}_3$  or  $\text{C}_2\text{H}_2\text{Cl}_2$ ) experimentally favoring the symmetric forms.<sup>25</sup> For both **1** and **2**, simulations were hence conducted on a single macrocyclic molecule at constant temperature using a Nosé thermostat.<sup>48</sup> The HREM simulations for compound **1** and **2** were done using a protocol<sup>23</sup> with scaling of all intramolecular interactions (except for stretching and bending) with  $s_{\min} = 0.1$  corresponding to a maximum “temperature” of 3000 K. We used eight or twelve states/replicas depending on the system, with scaling protocol given by  $s_k = s_{\min}^{(k-1)/(n-1)}$  and an EAF of  $20 \text{ ps}^{-1}$ . HREM produced 16 ns on the target state, for a total of 128 ns or 192 ns of simulations. In a second series of

HREM simulations on compounds **1** and **2**, the scaling protocol was optimized in the first 1.6 ns by balancing the acceptance ratio on the fly using the iterative scheme of Eq. 4 ( $c = 2$  and  $\omega = 1/160$  ps<sup>-1</sup> with ten iteration cycles).

For the ODR-BRD4(I) complex, starting from the 3SVG PDB structure we performed a pre-equilibration stage at the constant pressure of 1 atm and constant temperature of 300 K for 1 ns in a cubic box containing  $\simeq 7500$  water molecules (modeled using the TIP3P potential).<sup>49</sup> Constant pressure was enforced using a Parrinello-Rahman Lagrangian for isotropic stress tensor.<sup>50</sup> Constant temperature was imposed using two Nosé thermostats coupled to the internal coordinates and center of mass coordinates of the molecules.<sup>48,50</sup> Long range electrostatics were treated using the Particle Mesh Ewald technique.<sup>51</sup> For the BRD4(I) complex we used a solute-tempering HREM with a “hot zone” including the ODR ligand and the nearby residues (namely MET43, TRP81, PHE83, GLN85, VAL87, LEU92, LEU94, TYR97, TYR139, ASN140, ASP145, ILE146, MET149). The HREM simulations was performed using 12 replicas for 24 ns on the target state (288 ns in total) with the standard scaling protocol  $s_k = s_{min}^{(k-1)/(n-1)}$  with  $s_{min} = 0.1$  and  $n = 12$ . In a second HREM simulation of the complex, acceptance ratio was balanced on the fly for the first 1.6 ns. In Eq. 4, we used  $c = 2$  and  $\omega = 1/160$  ps<sup>-1</sup> with ten iteration cycles.

All simulations were performed using the program ORAC6.1<sup>52</sup>

## 4 Results

### 4.1 Compound 1: induced fit

Compound **1** adapts its conformation to the binding guest via an induced fit mechanism.<sup>25</sup> In Fig. 2 we show the two main conformations of macrocycle **1**. The two cage structures can be distinguished by the value of any of the three angles  $\alpha$  involving equivalent phenyl carbons (in orange color) on the three sides of the cage. In the most symmetric conformer **a** (on the left in Figure 2) the three angles are in the range 55-70 degrees, while in the twisted structure **b** (on the right in Figure 2), one of the angles is around 45 degrees. One of the two rapidly exchanging conformations is in general selected when **1** bind specifically to quarternary ammonium cations.<sup>25</sup>

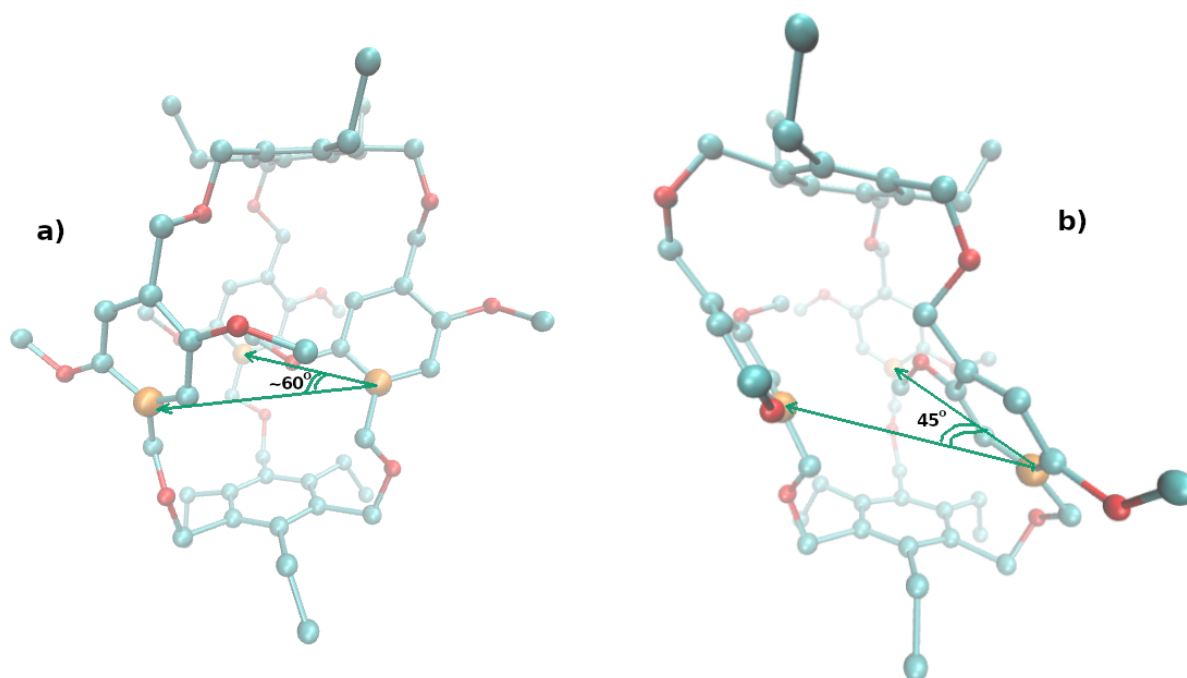


Figure 2: Main conformers in compound **1** in the gas-phase

#### 4.1.1 HREM simulations

We performed two HREM simulations, each lasting 16 ns, of the compound **1** *in vacuo* at 300 K. In both cases, due to the relatively low conformational barriers between the two structure (see Figure 6 further on) , we used only eight replicas and a minimum scaling factor of 0.1. In one of the HREM simulations, the scaling protocol was given by Eq. 3. In the other, we used the acceptance ratio balancing algorithm of Eq. 4 starting from the default scaling protocol of Eq. 3. In Table 2, we report the acceptance probability (in percent) for the HREM simulations with and without  $P_{acc}$  balancing. In the standard HREM simulation, with the default scaling Eq. 3,  $P_{acc}$  balance is poor,

Table 1: Acceptance probability (%) for the unbalanced and balanced HREM simulations in compound **1**

Eq. 4	1 ↔ 2	2 ↔ 3	3 ↔ 4	4 ↔ 5	5 ↔ 6	6 ↔ 7	7 ↔ 8
no	2.6	3.3	7.6	12.5	18.4	25.7	32.9
yes	8.0	10.5	12.4	12.7	11.8	11.2	11.4

with  $P_{acc}$  at the end of the ladder being more than one order of magnitude larger with respect to

exchanges  $1 \leftrightarrow 2$  involving the target state. In the adaptive HREM simulation, excellent balancing was reached after ten iteration of Eq. 4 (taken at regular interval in the first 1.6 ns simulation) at the expense of the mean acceptance ratio which dropped from 14.4% to 11.2 %.

As shown in ref.,<sup>42</sup> well balanced acceptance ratio, while avoiding bottlenecks in the replica diffusion, do not guarantee efficient HREM sampling in conformationally complex systems. Sampling efficiency can be assessed precisely by evaluating the replica flux, Eq. 2, strictly related to the mean round trip times (RTT) in the two HREM simulations. An estimate of the flux is evaluated, rather than directly using the slowly convergent Eq. 2, using the approach described in Ref.<sup>42</sup> based on the mean first passage times (MFPT) *within* the scaling factor ladder (see Eq. 6-11 of Ref.<sup>42</sup>). In the latest ORAC beta distribution,<sup>52</sup> (publicly available on <https://zenodo.org/record/8224111>) we provide a simple `awk` script, `replica_flux.awk`, to compute the flux in HREM using the MFPT approach proposed by Nadler *et al.*<sup>42</sup> In Figure 3, we report the flux as a function of the nodes for the HREM simulations sampled during the 16 ns HREM simulations with (green) and without (dark green) the balancing of the scaling factors according to Eq. 4. As the figure shows, the equalization of the acceptance ratio using Eq. 4 produced only a modest improvement on the flux.

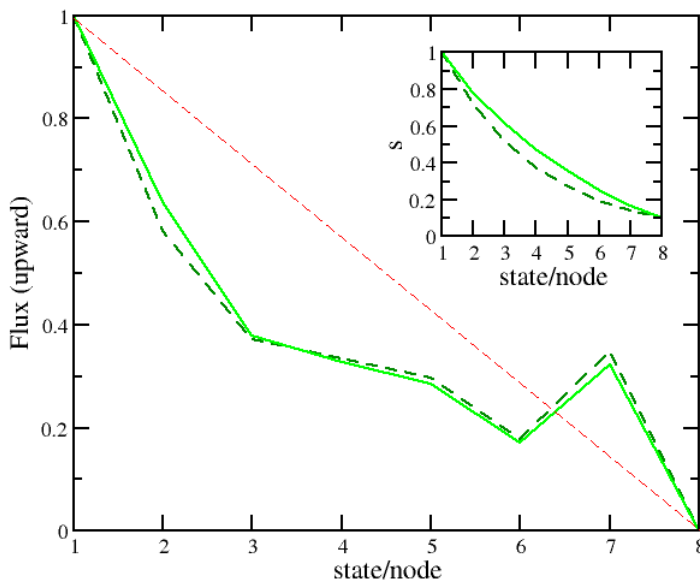


Figure 3: Upward flux (Eq. 2) in the HREM simulations of compound 1 estimated using the MFPT (see text). Dashed dark green: standard HREM with fixed scaling (Eq. 3). Solid green: HREM with iterative acceptance ratio balancing (Eq.4). In the inset we report the scaling factors as a function of the nodes with and without the adaptive scheme of E. 4

The mean absolute deviation with respect to the ideal flux is 0.15 and 0.16 for the balanced and unbalanced HREM simulation, evidencing the fact that well behaving short-time properties such as  $P_{acc}$  equalization do not necessarily imply an ideal or near-to-ideal flux across the replica progression.<sup>42</sup> Efficiency of the flow in a HREM simulation can also be assessed by measuring the fraction of the total simulation time that a replica spends on a given state. Ideally, each replica should spend the same fraction of time on each node/state given by  $\tau(k) = 1/n$ . Deviation from the ideality can be measured by evaluating the quantity

$$\mathcal{S}(k) = n \sum_i^n \tau_i^2(k) - 1 \quad (6)$$

where the sums are on all replica walkers (8 in our case).  $\mathcal{S}(k)$  corresponds to the variance of the variable  $\tau_i(k)/(1/n)$  expressing the ratio between the observed and ideal fraction of time the  $i$ -th replica walker have spent on the node  $k$ . Ideally  $\mathcal{S}(k) = 0 \quad \forall k$ . In Figure 4 we show the results

obtained in the two HREM simulations. The variance  $\mathcal{S}(k)$  are similar with no significant gains when using the adaptive scheme based on  $P_{\text{acc}}$  equalization, hence confirming the moderate impact of  $P_{\text{acc}}$  on-the-fly balancing on replica flow.

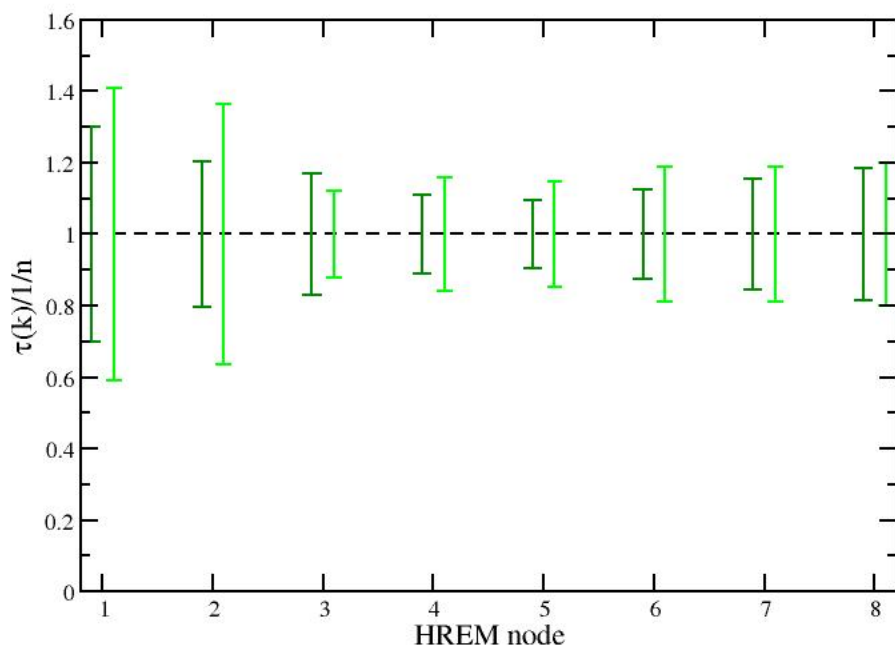


Figure 4: Variance as a function of the node index of the ratio  $\tau(k)/(1/n)$  (see text) in unbalanced (dark green) and balanced (green) HREM simulations of compound 1

Metrics for the two HREM simulation are finally collected in Table 2.

Table 2: HREM metrics with and without  $P_{\text{acc}}$  balancing in compound 1.

Eq. 4	$N_{\text{rep}}$	$s_{\text{min}}$	$\langle P_{\text{acc}} \rangle$ (%)	$\delta P_{\text{acc}}$	RTT/ns	$\Delta f_{\text{up}}$	$\langle \mathcal{S} \rangle^{1/2}$
no	8	0.1	14.7	10.6	0.71	0.16	0.16
yes	8	0.1	11.2	1.4	0.62	0.15	0.22

As it can be seen, notwithstanding the fact that the standard deviation of the of  $P_{\text{acc}}$  is reduced by one order of magnitude,  $P_{\text{acc}}$  balancing has a marginal positive effect on the RTT and the deviation from the ideal flux  $\Delta f_{\text{up}} = \frac{1}{n-1} \sum_k f(k) - (1 - k/n)$ , and a negative effect on the mean acceptance ratio and  $\langle \mathcal{S} \rangle$ . The benefit of ratio balancing via E. 4 for the replica flow is very likely negatively

compensated by the significant decrease of the balanced mean acceptance ratio.

In Fig. 5, we show the time record of the angle  $\alpha$  in the target state for two HREM simulations lasting 16 ns. Unlike in standard MD (see Fig. 8 further on), the swaps between the two conformations are frequent. In the HREM simulation with on-the-fly balancing of the acceptance ratio (bottom plot), swaps between the twisted and symmetric conformation appear to occur more frequently.

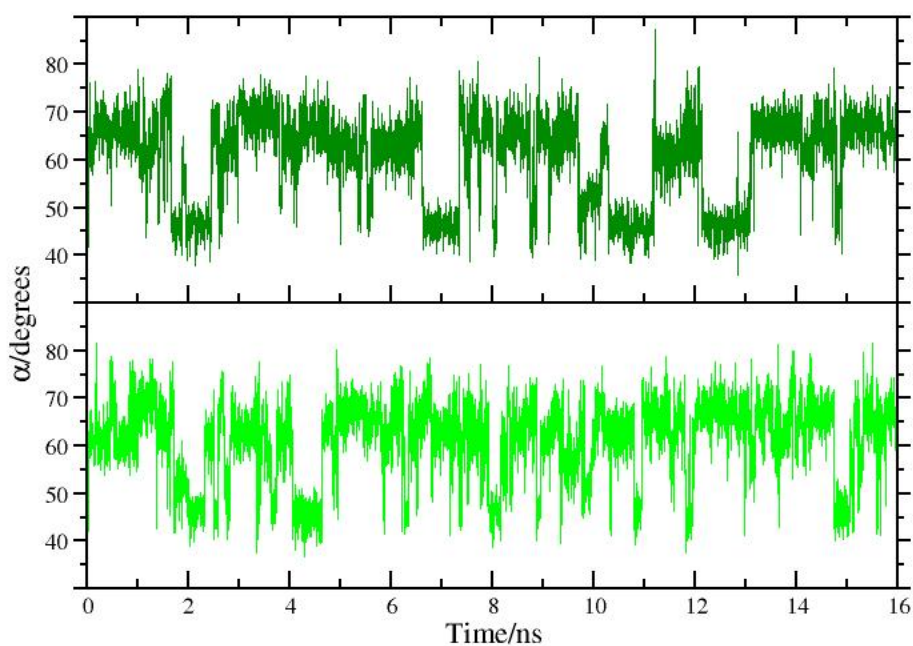


Figure 5: Time record of the  $\alpha$  angle (see Fig. 2 in a HREM simulation with fixed scaling of Eq. 3 (dark green) and with adaptive scaling according to Eq. 4 (green).

We finally examine the effect of Eq. 4 in the two HREM simulations with respect to the free energy difference between the two conformations of compound **1**, a quantity that is highly relevant for host-guest binding free energy calculations. To this end, in the Figure 6a we report calculated the potential of mean force (PMF) along the  $\alpha$  coordinate computed as  $V_{\text{PMF}}(\alpha) = -RT \ln(P(\alpha)/\max(P(\alpha)))$  where  $P(\alpha)$  is the probability distribution of *one* of the three equivalent angles  $\alpha$  defined by the three atoms highlighted in Figure 2 during the simulation of the gas-phase molecule. The green and dark green curves refer to the HREM simulation with and without  $P_{\text{acc}}$

balancing, respectively.

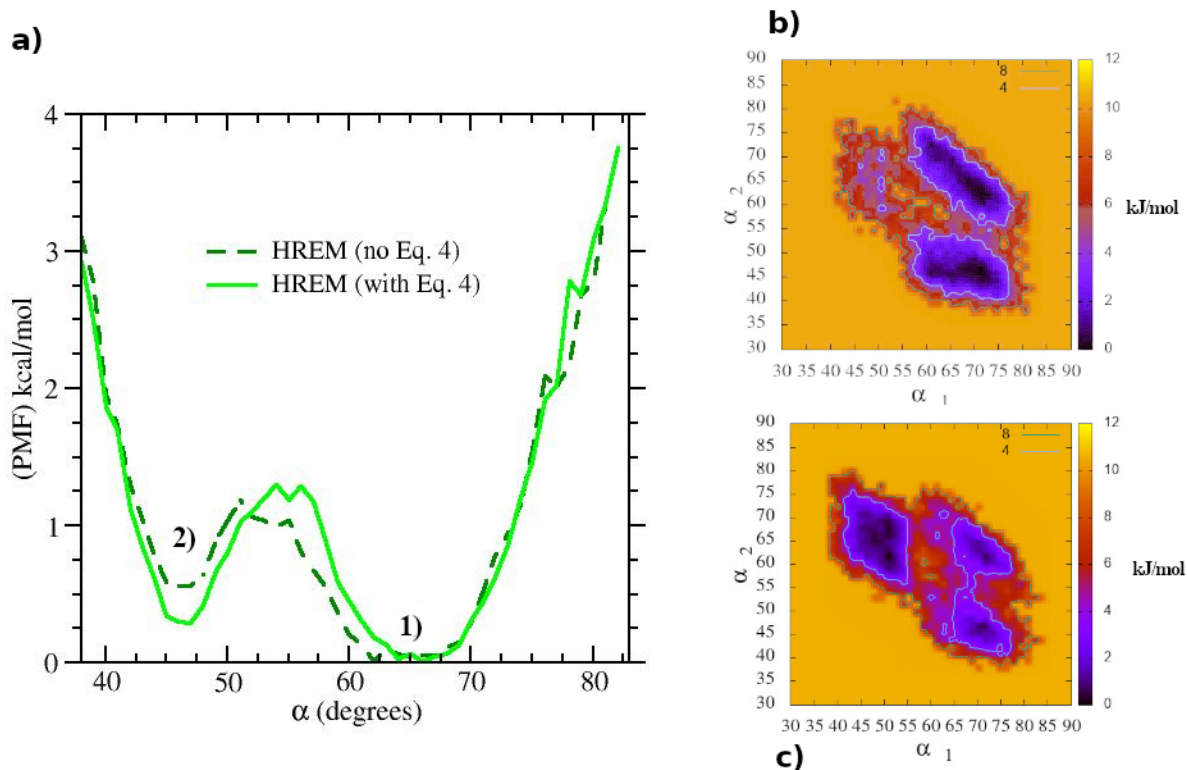


Figure 6: a) Potential of mean force along the  $\alpha$  angle in compound 1; Green-dashed: standard HREM green: HREM with acceptance ratio balancing. The minima labeled 1) and 2) correspond to the structures of compound 1 shown in Fig. 2. 2D PMF as a function of two angles (see text) computed by way HREM without (b) and with (c) acceptance ratio balancing.

The two minima in the HREM simulations (referring to the symmetric and twisted conformations) differ by less than 0.2 kcal/mol, separated by a barrier of about 1 kcal/mol. The quality of the sampling in the two HREM simulations can be further assessed by evaluation of the 2-dimensional PMF with respect to *any* pair of the angles of the triangle defined by the three atoms highlighted in Figure 2. Due to quasi- $C_{3h}$  symmetry of the structure 1 in Figure 2, we expect three minima for the cumulative 2D PMF with respect to any pair, with two equivalent minima with one angle of 45 degrees corresponding to the twisted structure and wide minimum with angles in the range  $\simeq 55-70$ . The 2D PMF are reported in Figure 6b and 6c for the standard and acceptance ratio balanced HREM simulation, respectively. The latter PMF is closer to the expected landscape, showing that the quality of sampling has been somewhat enhanced by the usage of Eq. 4.

### 4.1.2 Standard MD simulations

In Figure 7 we show the time records of one of the three the  $\alpha$  angle (see Figure 2) in a standard MD lasting for 128 ns, i.e. using the same amount of CPU time of the HREM simulations. No abrupt changes of the angle are observed during the first 50 ns of simulation implying that no flipping of the two involved phenyl moieties has taken place during this time. Flipping in the first 50 ns do occur only on the third phenyl side probed by the other two  $\alpha$  angles (data not shown). Note that phenyl flipping as probed by the angle occurs only three times during the whole 128 ns time span, in striking contrast (see Figure 5) with the two HREM simulations where many angle swaps are observed in the target state in only 16 ns of sampling.

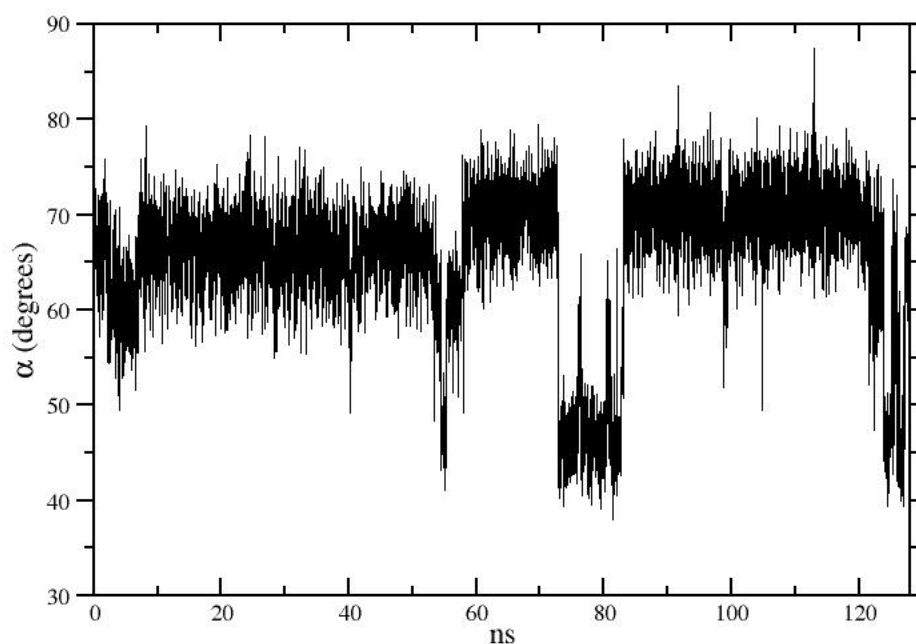


Figure 7: Time record of the  $\alpha$  angle in compound 1 (see Fig. ?? in a 128 ns standard MD simulation)

As authoritatively noted more than two decades ago, “individual [long MD] trajectories sample only a fraction of the conformational distribution generated by ten [much shorter] independent MD trajectories”.<sup>53</sup> This fact can be understood by considering that, while a single long trajectory may get stuck in one of the conformational attractors for a long time before it can jump to a different

conformational state, many short trajectories started from infinitesimally different initial conditions have a better chance of concurrently sampling several attractors.<sup>32,36</sup>

In Figure 8, we show the time record of one of the three equivalent angles in the triangle of Figure 2 for eight *replicates* of standard MD simulations of compound **1** each lasting 16 ns, with a cumulative sampling time of 128 ns, i.e. the same amount of time of the standard MD simulation of Figure 7.

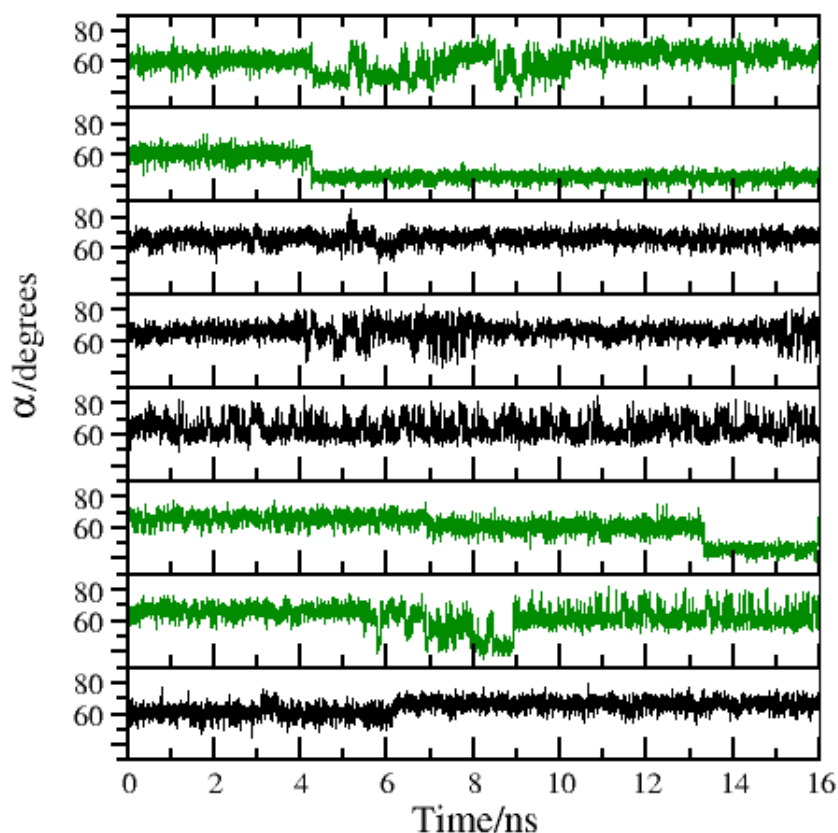


Figure 8: 8 replicates of 16 ns MD simulation of compound **1**

The rare event of the switching of the two conformations as probed by one of the  $\alpha$  has been observed six times in the cumulative 128 ns, compared to the three times only observed in the standard MD simulation of Figure 7.

In Figure 16 we report the PMF with respect to the  $\alpha$  angle obtained with standard MD simulations. For comparison we also included in the plot the PMF obtained using HREM with acceptance ratio balancing. None of the approaches based on standard MD is apparently able to produce reliable Boltzmann weights for the two conformations of compound **1** whose binding is characterized by the induced fit mechanism. We recall that in alchemical free energy simulations, a correct sampling of the *apo* state, or of states with small alchemical coupling, is an essential requirement for delivering reliable binding free energies. Phenyl flipping in compound **1** as probed by  $\alpha$  never occur in a standard 16 ns MD simulations, while is severely undersampled by extending the simulation up to 128 ns. The best results (i.e. those the are close those obtained with the two HREM simulations) are obtained using 16 ns replicates of standard MD simulations confirming the moderate effectiveness of this straightforward enhanced sampling approach.<sup>32,36</sup>

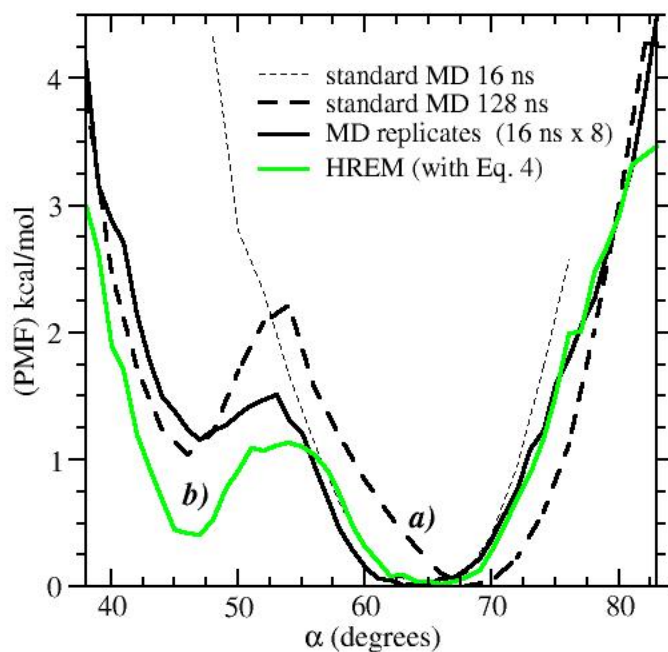


Figure 9

Figure 10: Potential of mean force along the  $\alpha$  angle in compound **1** computed using standard molecular dynamics simulations (black color) and HREM using Eq. 4 (green color).

## 4.2 Compound 2: conformational selection

Compound **2** is characterized by two non equivalent couples of stacked naphthyl moieties whose flipping is regulated by torsions around two carbon-carbon  $sp_3$  bonds connected in one case to amide and in the other case to methylene moieties (see Figure 11). Because of the bulky naphthyl sides, torsional barriers for the switching between conformers are in the case of compound **2** much higher than they are in compound **1** with phenyl groups, hence giving rise to long-lived meta-stable conformational states determining the conformational selectivity of this host molecule.<sup>26</sup>

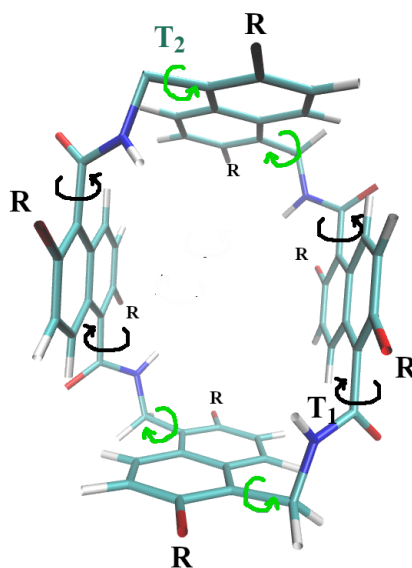


Figure 11: Compound **2** in configuration I with  $C_2$  symmetry.<sup>26</sup> The torsions around  $sp_3$  bonds connecting methylene or amide moieties are shown in green and black colors, respectively.

### 4.2.1 HREM simulations

Due to the presence of higher torsional barriers, the HREM simulation of compound **2** *in vacuo* required a minimum of 12 replicas with a minimum scaling factor of  $s_{\min} = 0.1$  to allow for at least one round trip on the average per replica during 16 ns of simulation. As for the case of compound **1**, we launched two 16 ns HREM simulations with and without on-the-fly balancing of the acceptance ratio according to Eq. 4 with the starting standard scaling protocol given by Eq. 3. In Figure 12

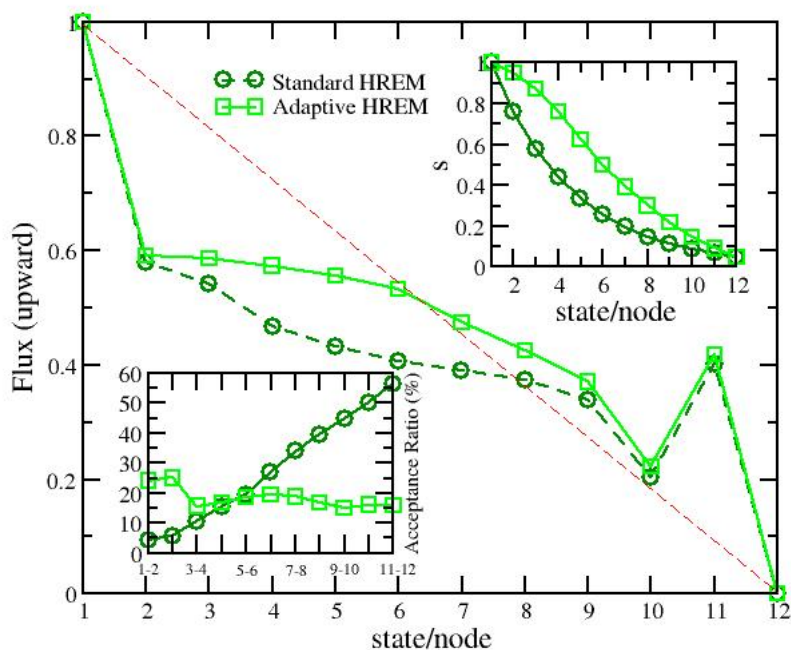


Figure 12: Upward flux (Eq. 2) in the HREM simulations of compound **2** estimated using the MFPT (see Sec 4.1.1). Dark green: standard HREM with fixed scaling (Eq. 3). Solid green: HREM with iterative acceptance ratio balancing (Eq.4). In the top-right inset we report the scaling factors as a function of the nodes with and without the adaptive scheme of Eq. 4. In the bottom left inset, we report the acceptance ratios with and without the adaptive scheme of Eq. 4.

we show the flux (Eq. 2), the acceptance ratio and the scaling protocols obtained with the standard (Eq. 3) and adaptive (Eq. 4) HREM approaches. As observed for the case of compound **1** (see Sec. 4.1.1), the use of the adaptive scheme Eq. 4 for acceptance ratio equalization leads to an overall decrease of the mean  $P_{acc}$  dropping to 18.3 from 28.0. Nonetheless, ratio equalization has a positive effect on the measured flux with a mean deviation from ideality ( $\Delta f_{up}$ ) decreasing to 0.11 from 0.14 of the standard HREM algorithm based on Eq. 3. Replica flow improvement with Eq. 4, while marginal for compound **1**, is significant in compound **2** where the torsional barriers for sidewall flipping are much higher than they are in the host **1** (see Figure 14 further on). As shown in Table 3,

Table 3: HREM metrics with and without  $P_{\text{acc}}$  balancing in compound **2**.

Eq. 4	$N_{\text{rep}}$	$s_{\text{min}}$	$\langle P_{\text{acc}} \rangle$ (%)	$\delta P_{\text{acc}}$	RTT/ns	$\Delta f_{\text{up}}$	$\langle \mathcal{S} \rangle^{1/2}$
no	12	0.1	28.0	17.5	2.68	0.14	0.39
yes	12	0.1	18.3	3.2	2.12	0.11	0.50

the adaptive algorithm in Eq. 4 has a positive and significant effect on the mean round trip time. In Table 3 we have collected the main metrics for the two HREM approaches in the simulation of compound **2**. The mean round-trip time is found to be 2.12 ns for the adaptive scheme, i.e. nearly 20% less than that obtained (2.68 ns) with the standard HREM scaling. Concerning the variance  $\mathcal{S}$  (Eq. 6) i.e. the mean deviation of the time spent on any given node/state by each walker with respect to the ideal fraction of 1/12, we observe an increase when using the adaptive scheme as already noticed for the case of compound **1** (see Table 2).

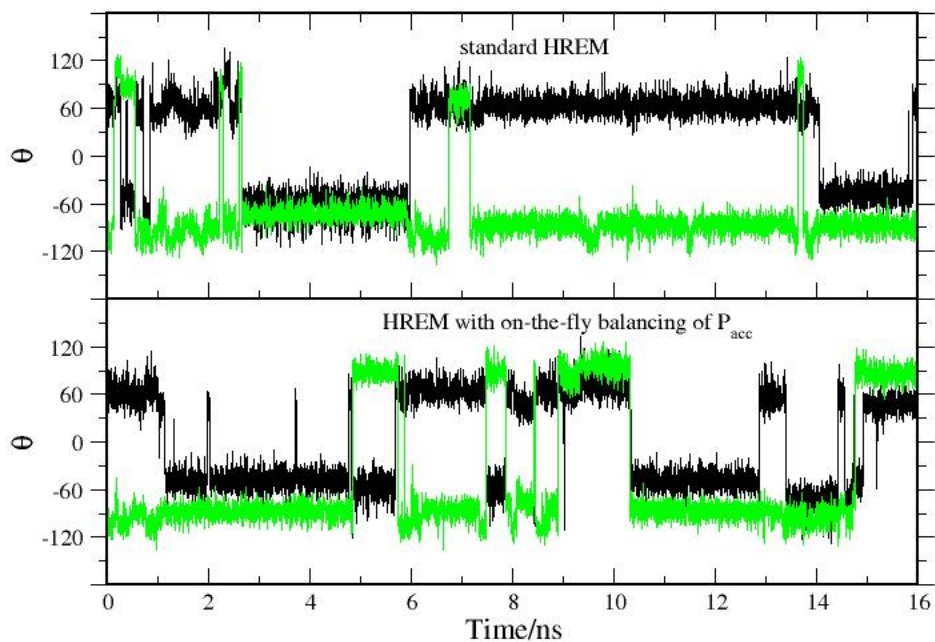


Figure 13: Time record of the  $T_1$  and  $T_2$  torsional angles (in degrees) in compound **2** (see Figure 11) for the HREM simulation with (bottom plot) and without (top plot) balancing of the acceptance ratio probability using Eq. 4

In Figure 13 we show the time record of the dihedral angles  $T_1$  and  $T_2$  (see Figure 11) regulating

the flipping of the two non equivalent naphthyl moieties in compound **2** using HREM with and without the adaptive scheme of Eq. 4. Flipping events are somewhat enhanced using the adaptive scheme.

In Figure 14 we finally show the PMF along the dihedral angles  $T_1$  and  $T_2$  obtained using the two HREM protocols in the simulation of compound **2**. The two PMFs are quite similar especially for the  $T_1$  torsion involving the naphthyl side walls connected by amide moieties (see Figure 11). For the  $T_2$  torsion, there are non-negligible discrepancies with the two minima differing by  $\simeq 1$  kcal/mol in the case of the HREM with the adaptive scheme of Eq. 4 and  $\simeq 1.5$  kcal/mol for the standard HREM simulation.

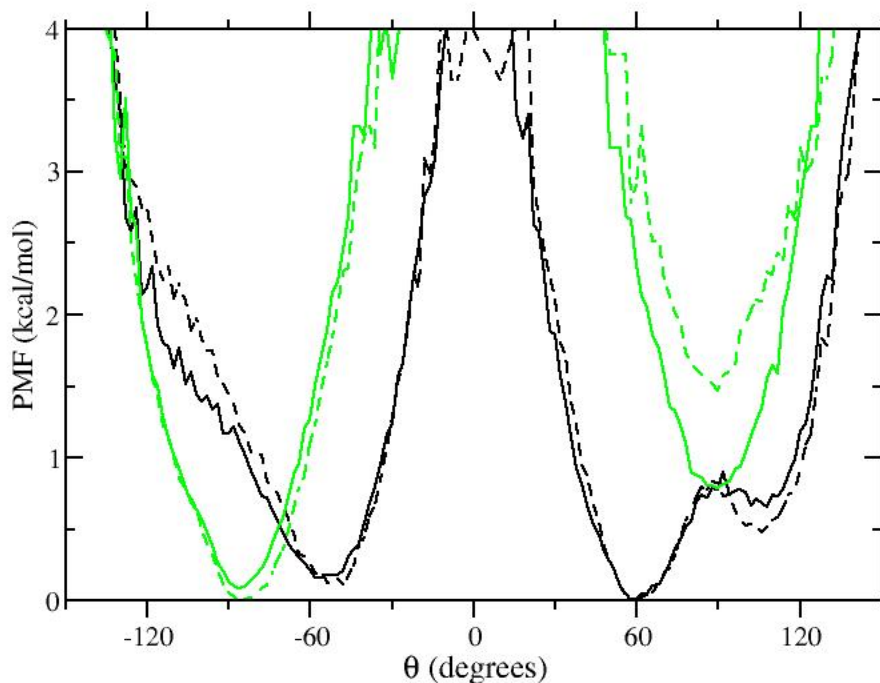


Figure 14: PMF of the  $T_1$  (black) and  $T_2$  (green) dihedral angles (see Figure 11) obtained with standard HREM (dashed lines) and with adaptive HREM using Eq. 4 for  $P_{acc}$  balance.

Given the better behavior of the flow and the shorter RTT's obtained in the case of HREM with the adaptive scheme, we can assume that the usage of Eq. 4 is somewhat improving the sampling efficiency, hence providing a more accurate PMF with respect to the  $T_2$  collective coordinate. As expected, the torsional barriers for the flipping of the naphthyl groups exceed in both cases 4

kcal/mol, hence giving rise to long lived meta-stable states in compound **2**. Quite surprisingly in both the HREM simulations, the higher barrier is detected for the  $T_2$  torsion involving the methylene moieties (see Figure 11).

#### 4.2.2 Standard MD simulations

In Figure 15, we show the time record of the  $T_1$  and  $T_2$  dihedral angles during a 128 ns long standard MD simulation of compound **2**. We observed *one* naphthyl flipping as probed by  $T_1$  and no flipping for the methylene connected naphthyl moieties, during the entire simulation. Standard MD is apparently unable to reliably sample the conformational states of compound **2** even extending the simulation time beyond 100 ns. In the bottom plot of Figure 15, we show, sequentially, the time record of the  $T_1$  and  $T_2$  dihedral angles obtained in 8 MD simulation replicates, each lasting 16 ns only. Flipping of the  $T_1$  torsion is observed in six

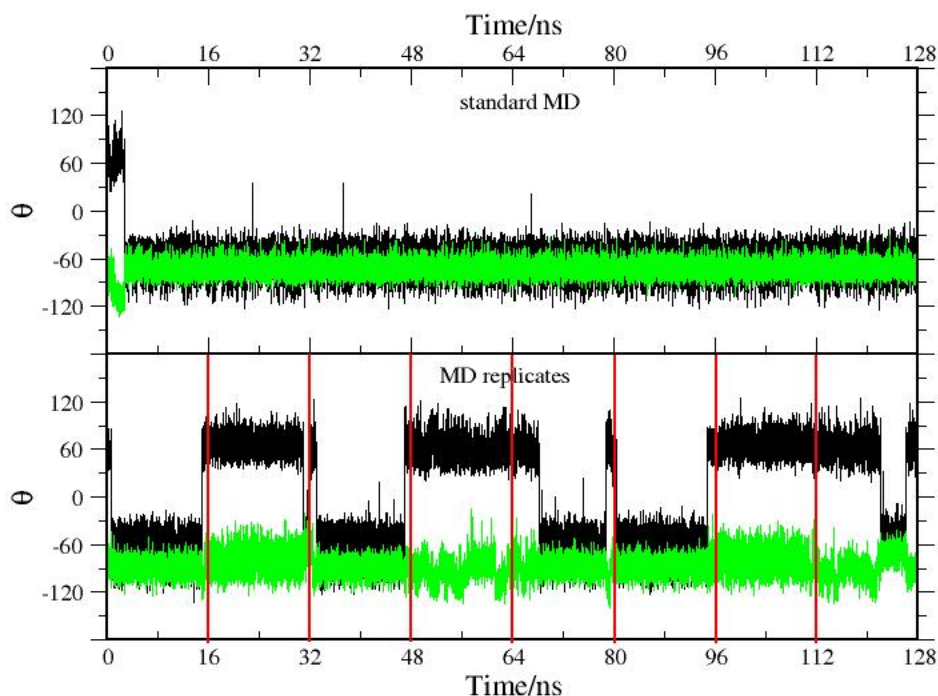


Figure 15: Time record of the  $T_1$  and  $T_2$  torsional angles (in degrees) in compound **2** (see Figure 11) for a standard MD simulation of 128 ns (top plot) and for 8 replicates of 16 ns standard MD (bottom plot). Red vertical lines mark the beginning/end of the MD replicates.

out of the eight replicates, while again the  $T_2$  dihedral is stuck to the initial value of  $\simeq -60^\circ$  in each of the replicates. The rare event of naphthyl flipping occurs, as observed for the phenyl flipping in compound **1**, in a sub-picosecond time scale.

In Figure 16 we finally show the PMF obtained for the torsional potential of the  $T_1$  (black color lines) and  $T_2$  (green color lines) dihedral angles using standard MD and replicates of much shorter standard MD simulations. In the Figure, the PMF obtained with the adaptive HREM (in blue and cyan color) is also superimposed for comparison. For the  $T_1$  torsion, characterized by a barrier of  $\simeq 5$  kcal/mol, we notice that the statistics collected in the 8 replicates MD simulations (128 ns in total) produces a PMF that closely follows that obtained with the 16 ns of HREM simulation. For the  $T_2$ , standard MD simulations, whether using short replicates or a single long lasting run, are unable to sample the secondary minimum detected in HREM at  $\theta = 60^\circ$ , showing the limitations of the straightforward replicates approach when dealing with long-lived meta-stable states.

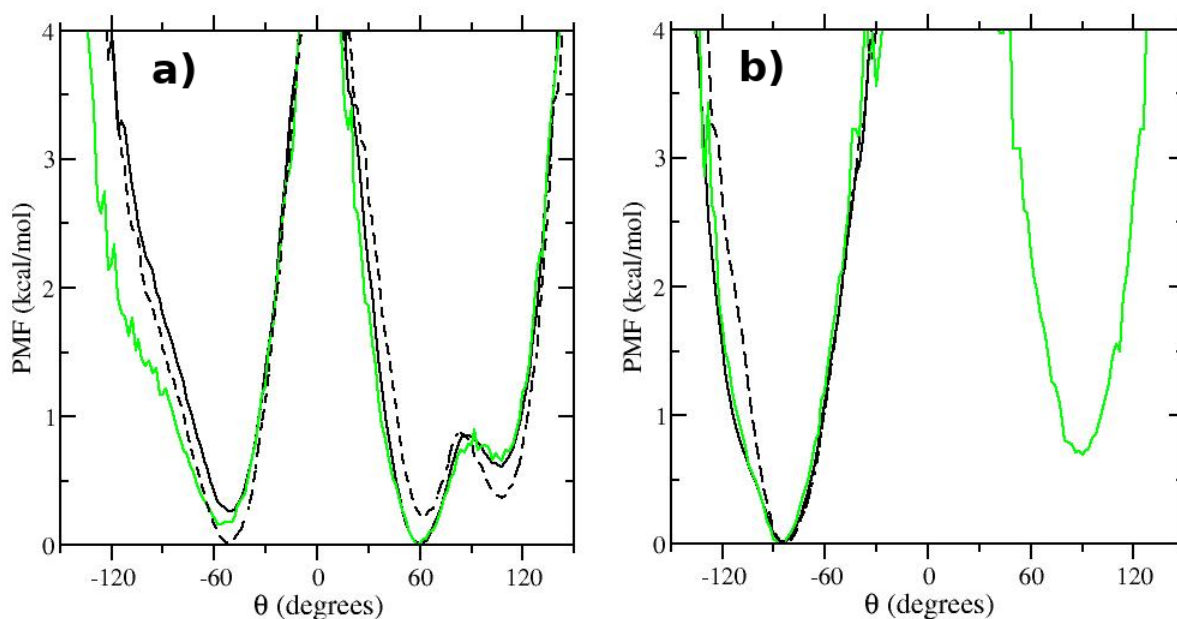


Figure 16: PMF of the  $T_1$  (a) and  $T_2$  (b) dihedral angles (see Figure 11) obtained with 128 ns long standard MD (dashed black line) and eight 16 ns long standard MD replicates (solid black line). The PMF obtained using the adaptive HREM simulation is shown in green.

### 4.3 BRD4(I) in complex with the ODR ligand

We finally compare conformational sampling using HREM, adaptive HREM (Eq. 4) and MD replicates for the simulation of the BRD4(I) in complex with the ligand ODR (see Figure 1). Technical details of the simulation are provided in Sec. 3.2. In Figure 17 we show the two main poses of the ODR ligand in the BRD4(I) scaffold sampled during the MD runs. Figure 17a refers to the crystallographic pose in the 3SVG PDB file. The pose on the left, with ODR rotated by  $\simeq 180^\circ$  around an axis passing through position 3, 6 of the central phenyl moiety in ODR, is observed in both HREM and MD replicates simulations.

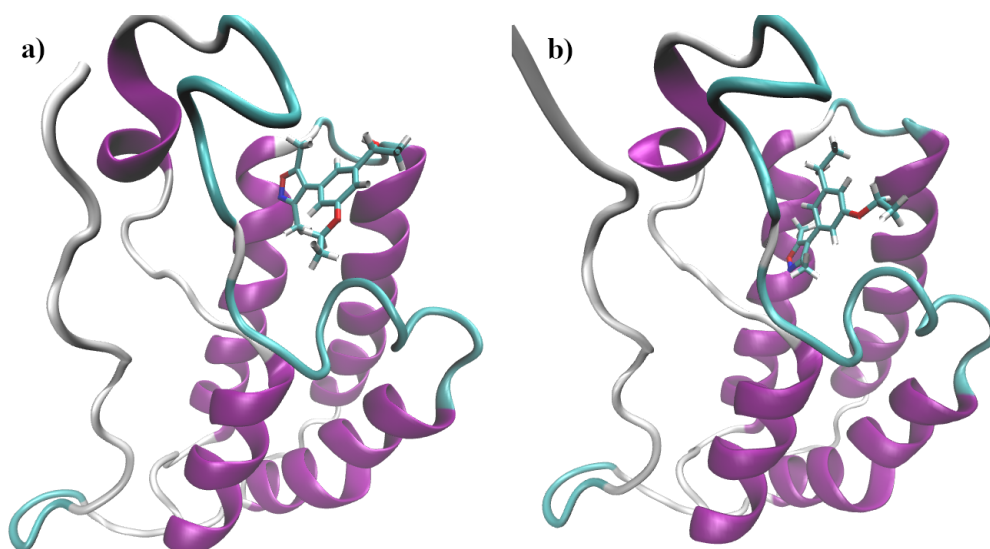


Figure 17: a) Crystallographic and primary pose of the ODR ligand in complex with BRD4(I); b) secondary pose of the ODR ligand sampled in the HREM and standard MD simulations

In Table 4, we have collected all relevant parameters for the HREM simulation of the ORD-BRD4(I) complex in explicit solvent. The sub-system, involved in 12-fold scaling down to  $s_{\min} = 0.1$ , includes the ligand and the hot-zone residues for a total of 183 atoms, comparable to the number of atoms in compound **2** (157), which was simulated using the same HREM protocol. As a trivial consequence of this fact, we observe the same pattern in the acceptance ratio using the standard scaling Eq. 3 in the the BRD4(I) complex and in compound **2** with  $P_{\text{acc}}(k)$  steadily

Table 4: HREM metrics with and without  $P_{\text{acc}}$  balancing in the complex of ODR-BRD4(I)

Eq. 4	$N_{\text{rep}}$	$s_{\text{min}}$	$\langle P_{\text{acc}} \rangle$ (%)	$\delta P_{\text{acc}}$	RTT/ns	$\Delta f_{\text{up}}$	$\langle \mathcal{S} \rangle^{1/2}$
no	12	0.1	29.1	13.3	1.60	0.14	0.36
yes	12	0.1	28.3	7.6	0.97	0.10	0.47

increasing with the node index  $k$  and with nearly identical mean values (29.1% for BRD4(I)-ODR and 28% for compound **2**). As observed for the HREM simulations of compound **2**, also in the case of the BRD4(I)-ODR complex, flux and RTT are improved by implementing the acceptance ratio balancing via Eq. 4. In the BRD4(I)-ODR complex we observe only a moderate degradation of the mean acceptance ratio upon ten cycles (during 1.6 ns) of implementing Eq. 4, at variance with what was observed in compounds **1** and **2** (see Tables 2 and 3). As in compound **1** and **2**, the variance  $\mathcal{S}$  (Eq. 6) increases when using Eq. 4.

In Figure 18

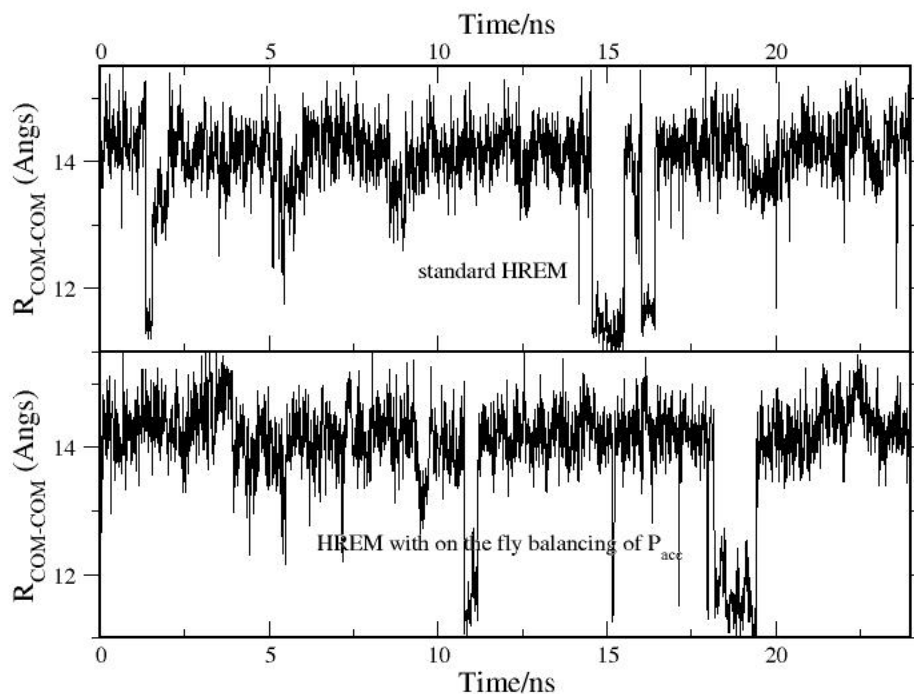


Figure 18: Time record of the distance between the center of mass of BRD4(1) and of ODR using standard HREM (top) and adaptive HREM using Eq. 4

we report the time record of the distance between the centers of mass of the ligand and the receptor ( $R_{\text{COM-COM}}$ ) obtained in the HREM simulation with and without the use of the adaptive scheme of Eq. 4 for  $P_{\text{acc}}$  balancing. The plot shows a clear prevalence of the crystallographic pose (see Figure 17a) characterized by  $R_{\text{COM-COM}} \simeq 14-15 \text{ \AA}$ . The secondary pose at  $R_{\text{COM-COM}} \simeq 11-12 \text{ \AA}$  (see Figure 17b) is sampled five and seven times in the standard and the adaptive HREM simulation, respectively, with a probability around 7% in both cases.

In Figure 19 we report the time record of 12 juxtaposed replicates of standard MD simulations each lasting 24 ns. The five magenta-highlighted replicates indicate independent 24 ns MD simulations where the secondary pose was never observed. The secondary pose was sampled 10 times in the total 288 ns time span of standard MD replicates, with a probability of 7% (as in HREM). In the bottom plot of Figure 19, we show a zooming of the 10th MD replicate where the pose switch was observed. Note that the duration of this rare event occurs in less than 200 ps, despite the fact that ligand must rotate by  $\simeq 180^\circ$  around the phenyl axis with a shift of the COM of nearly 3  $\text{\AA}$ . Again, we are dealing also in this case with a rare event that occurs on a fast time-scale.

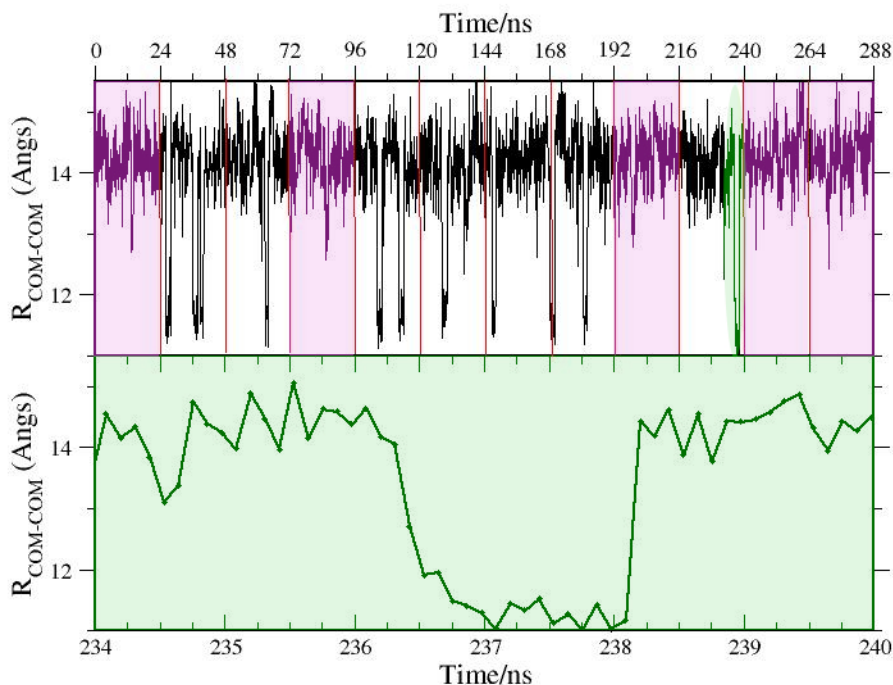


Figure 19: Time record of the distance between the center of mass of BRD4(1) and of ODR using 12 replicates of standard MD simulation, each lasting 24 ns

In Figure 20 we finally compare the probability distribution (and the associated PMF) of the poses of the ODR ligand in the BRD4(I) complex obtained in HREM and using MD. Inspection of Figure 20a shows that standard and adaptive HREM produces essentially the same probability profile and PMF. This probability and PMF can only be recovered using 12 replicates of MD (for a total of 288 ns), while a simple 24 ns vanilla simulation (first of the 12 replicates in Figure 19) is missing completely the sampling of the secondary pose.

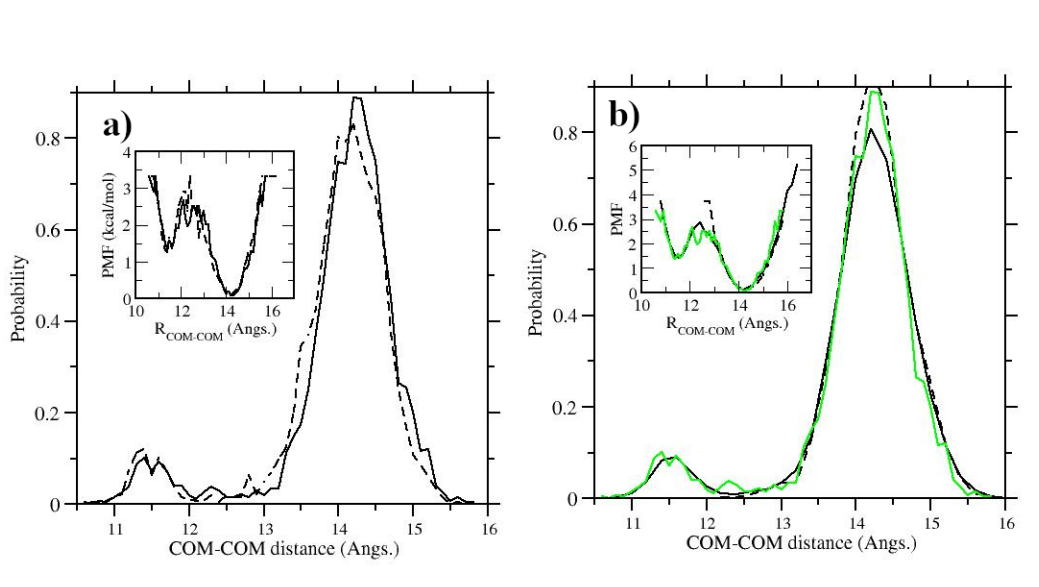


Figure 20: a) Ligand-receptor COM-COM distance distribution and associated PMF (in the inset) using standard HREM (dashed line) and HREM with adaptive scaling using Eq. 4 (solid line). HREM simulation lasted in both cases 24 ns; b) Ligand-receptor COM-COM distance distribution and associated PMF (in the inset) obtained with a 24 ns standard MD (dashed line) and with 12 replicates of 24 ns MD simulations (solid lines). In green we show the distribution obtained with the adaptive HREM

If on one hand it is indeed encouraging that MD replicates are able to collectively sample the two ligand poses with the same probability obtained in HREM simulations investing the same amount of CPU time, on the other hand it is quite disheartening that we needed, in total, 288 ns of standard MD simulation for such result. In a FEP approach, there is no reason to believe that such amount of time is required *only* to sample effectively the initial state of the ligand-receptor complex. If we change the nature of the ligand-receptor interactions, as it occurs in the alchemical intermediate states of a standard FEP calculation, we very likely alter the probability ratio of the two poses, with an impact on the free energy change. For example, the oxygen of the isoaxazole moiety of ODR is engaged in a strong hydrogen bond with a hydrogen of the  $\text{NH}_2$  group of ASN100 in the primary

pose. This H-bond is lost when the ligand switches to the secondary pose. Hence, when, e.g., the electric charges on the alchemical ligand are turned off as commonly done in a FEP calculations where electrostatic and Lennard-Jones interaction are sequentially switched off, the probability ratio of the two main poses in the BRD4(I)-ODR complex is likely to change significantly, with a direct effect on the free energy change.

In the MD-based alchemical approach for drug design, a simple way of overcoming such stumbling blocks in the sampling of complex conformational landscapes of hosts or ligand receptor systems is that of limiting the enhanced sampling simulations to the sampling of the end-states only, and then connecting these end-states by a swarm of fast (few ns at most) nonequilibrium (NE) alchemical simulations,<sup>38,54,55</sup> recovering the free energy change from the resulting NE work distribution using the Jarzynski<sup>56</sup> or the Crooks theorems.<sup>57</sup> This approach, by forcing the occurrence of fast rare events exploiting the replica diffusion in the scaling ladder or the sampling efficiency of many short and independent MD replicates on parallel platforms, in some sense restores the thermodynamics, hence avoiding to rely on an often unattainable ergodicity on *each* intermediate alchemical state in a *single* extended simulation of a *single* molecular systems characterized by a rugged free energy landscape.

## 5 Conclusion

We have performed extended MD simulations using Hamiltonian Replica Exchange and standard MD on two macrocyclic hosts, compound **1** (see Figure 2) and compound **2** (see Figure 11) that selectively bind small guest molecules via an induced fit and a conformational selection mechanism, respectively. HREM and MD simulations have been also performed on the ODR-BRD4(I) complex in TIP3 water, with the ligand occupying two competing poses (see Figure 17). In all cases, we used standard HREM based on the scaling protocol defined in Eq. 3 and an adaptive HREM with on-the-fly balancing of the acceptance ratio as provided by Eq. 4. Adaptive HREM seems to have a moderate positive impact on the average round-trip-time and on the replica flux, resulting in an improved sampling efficiency. “One off” MD simulations, even with a total simulation time exceeding by one order of magnitude that of the HREM simulations, are unable to reliably sample the

conformational space in the two macrocyclic hosts and in BDR4(I)-ODR complex. By distributing the total simulation time in a series of short independent standard MD replicates, the sampling efficiency is restored in the case compound **1** and in the BRD4(I)-ODR complex where conformational sub-states or secondary poses are separated by free energy barriers not exceeding 1-2 kcal/mol. For compound **2**, characterized by long-lived meta-stable structures separated by barrier exceeding 4 kcal/mol, HREM appears to be the only viable alternative for a reliable canonical sampling. The present results shows that in complex systems with a manifold of possible conformations, a fully converged and reproducible FEP-based approach would require costly HREM simulations on *each* of the intermediate alchemical states. This severe sampling issue can be in part circumvented by limiting the enhanced sampling to the end-states alone (the complex with the fully coupled ligand and the receptor in the **apo** structure) and recovering the binding free energy via nonequilibrium fast alchemical transformations connecting these end states.

## Data and Software Availability

PDB trajectory files from MD and HREM simulation (target state only), ORAC input files and force field parameter files are available at the general-purpose open-access repository Zenodo (<https://zenodo.org/record/8224111>) A beta version of the ORAC program with implementation of Eq. 4 in the **rem** module is also provided as a compressed **tar** archive in the same Zenodo repository.

## Acknowledgement

The computing resources and the related technical support used for this work have been provided by CRESCO/ENEAGRID High Performance Computing infrastructure and its staff. CRESCO/ENEAGRID High Performance Computing infrastructure is funded by ENEA, the Italian National Agency for New Technologies, Energy and Sustainable Economic Development and by Italian and European research programmes (see [www.cresco.enea.it](http://www.cresco.enea.it) for information). The author thanks MIUR-Italy (“Progetto Dipartimenti di Eccellenza 2023-2027” allocated to Department of Chemistry “Ugo

Schiff”) and the National Recovery and Resilience Plan, Mission 4 Component 2 - Investment 1.4 - NATIONAL CENTER FOR HPC, BIG DATA AND QUANTUM COMPUTING - funded by the European Union - NextGenerationEU - CUP B83C22002830001.

## References

- (1) Sink, R.; Pecar, S.; Zega, A. False Positives in the Early Stages of Drug Discovery. *Curr. Med. Chem.* **2010**, *17*, 4231–4255.
- (2) Deng, N.; Forli, S.; He, P.; Perryman, A.; Wickstrom, L.; Vijayan, R. S. K.; Tiefenbrunn, T.; Stout, D.; Gallicchio, E.; Olson, A. J.; Levy, R. M. Distinguishing Binders from False Positives by Free Energy Calculations: Fragment Screening Against the Flap Site of HIV Protease. *J. Phys. Chem. B* **2015**, *119*, 976–988, PMID: 25189630.
- (3) Wang, L.; Wu, Y.; Deng, Y.; Kim, B.; Pierce, L.; Krilov, G.; Lupyan, D.; Robinson, S.; Dahlgren, M. K.; Greenwood, J.; Romero, D. L.; Masse, C.; Knight, J. L.; Steinbrecher, T.; Beuming, T.; Damm, W.; Harder, E.; Sherman, W.; Brewer, M.; Wester, R.; Murcko, M.; Frye, L.; Farid, R.; Lin, T.; Mobley, D. L.; Jorgensen, W. L.; Berne, B. J.; Friesner, R. A.; Abel, R. Accurate and Reliable Prediction of Relative Ligand Binding Potency in Prospective Drug Discovery by Way of a Modern Free-Energy Calculation Protocol and Force Field. *J. Am. Chem. Soc.* **2015**, *137*, 2695–2703.
- (4) Gapsys, V.; Perez-Benito, L.; Aldeghi, M.; Seeliger, D.; van Vlijmen, H.; Tresadern, G.; de Groot, B. L. Large scale relative protein ligand binding affinities using non-equilibrium alchemy. *Chem. Sci.* **2020**, *11*, 1140–1152.
- (5) Cournia, Z.; Allen, B. K.; Beuming, T.; Pearlman, D. A.; Radak, B. K.; Sherman, W. Rigorous Free Energy Simulations in Virtual Screening. *J. Chem. Inf. Model.* **2020**, *60*, 4153–4169.
- (6) Özen, A.; Perola, E.; Brooijmans, N.; Kim, J. *Free Energy Methods in Drug Discovery: Current State and Future Directions*; American Chemical Society, 2021; Chapter 5, pp 127–141.
- (7) Jorgensen, W. L.; Buckner, J. K.; Boudon, S.; TiradoRives, J. Efficient computation of absolute free energies of binding by computer simulations. Application to the methane dimer in water. *J. Chem Phys.* **1988**, *89*, 3742–3746.
- (8) Zwanzig, R. W. High-temperature equation of state by a perturbation method. I. Nonpolar gases. *J. Chem. Phys.* **1954**, *22*, 1420–1426.

- (9) Bennett, C. H. Efficient estimation of free energy differences from Monte Carlo data. *J. Comp. Phys.* **1976**, *22*, 245–268.
- (10) Kirkwood, J. G. Statistical mechanics of fluid mixtures,. *J. Chem. Phys.* **1935**, *3*, 300–313.
- (11) Pohorille, A.; Jarzynski, C.; Chipot, C. Good Practices in Free-Energy Calculations. *J. Phys. Chem. B* **2010**, *114*, 10235–10253.
- (12) Procacci, P. Alchemical determination of drug-receptor binding free energy: Where we stand and where we could move to. *J. Mol. Graph. and Model.* **2017**, *71*, 233–241.
- (13) Wang, L.; Deng, Y.; Knight, J. L.; Wu, Y.; Kim, B.; Sherman, W.; Shelley, J. C.; Lin, T.; Abel, R. Modeling Local Structural Rearrangements Using FEP/REST: Application to Relative Binding Affinity Predictions of CDK2 Inhibitors. *J. Chem. Theory Comput.* **2013**, *9*, 1282–1293.
- (14) Caleman, C.; van Maaren, P. J.; Hong, M.; Hub, J. S.; Costa, L. T.; van der Spoel, D. Force Field Benchmark of Organic Liquids: Density, Enthalpy of Vaporization, Heat Capacities, Surface Tension, Isothermal Compressibility, Volumetric Expansion Coefficient, and Dielectric Constant. *J. Chem. Theory Comput.* **2012**, *8*, 61–74.
- (15) Zhang, H.; Yin, C.; Jiang, Y.; van der Spoel, D. Force Field Benchmark of Amino Acids: I. Hydration and Diffusion in Different Water Models. *J. Chem. Inf. Model.* **2018**, *58*, 1037–1052.
- (16) Mobley, D. L.; Bannan, C. C.; Rizzi, A.; Bayly, C. I.; Chodera, J. D.; Lim, V. T.; Lim, N. M.; Beauchamp, K. A.; Slochower, D. R.; Shirts, M. R.; Gilson, M. K.; Eastman, P. K. Escaping Atom Types in Force Fields Using Direct Chemical Perception. *J. Chem. Theory Computat.* **2018**, *14*, 6076–6092, PMID: 30351006.
- (17) Mobley, D. L. Let’s get honest about sampling. *J. Comput. Aided Mol. Des.* **2012**, *26*, 93–95.
- (18) Procacci, P. Solvation free energies via alchemical simulations: let’s get honest about sampling, once more. *Phys. Chem., Chem. Phys.* **2019**, *25*, 13826–13834.

- (19) Koshland, D. E. Application of a Theory of Enzyme Specificity to Protein Synthesis. *Proc. Natl. Acad. Sci.* **1958**, *44*, 98–104.
- (20) Monod, J.; Wyman, J.; Changeux, J.-P. On the nature of allosteric transitions: A plausible model. *J. Mol. Biol.* **1965**, *12*, 88–118.
- (21) Motlagh, H. N.; Wrabl, J. O.; Li, J.; Hilser, V. J. The ensemble nature of allostery. *Nature* **2014**, *508*, 331–339.
- (22) Sugita, Y.; Okamoto, Y. Replica-exchange molecular dynamics method for protein folding. *Chem. Phys. Lett.* **1999**, *314*, 141–151.
- (23) Marsili, S.; Signorini, G. F.; Chelli, R.; Marchi, M.; Procacci, P. ORAC: A Molecular Dynamics Simulation Program to Explore Free Energy Surfaces in Biomolecular Systems at the Atomistic Level. *J. Comput. Chem.* **2010**, *31*, 1106–1116.
- (24) Wang, L.; Friesner, R. A.; Berne, B. J. Replica Exchange with Solute Scaling: A More Efficient Version of Replica Exchange with Solute Tempering (REST2). *J. Phys. Chem.* **2011**, *115*, 9431–9438, PMID: 21714551.
- (25) Huang, Q.-C.; Quan, M.; Yao, H.; Yang, L.-P.; Jiang, W. Selective Recognition of Quaternary Ammonium Ions by Structurally Flexible Cages. *Chinese J. Chem.* **2021**, *39*, 1593–1598.
- (26) Yang, L.-P.; Zhang, L.; Quan, M.; Ward, J. S.; Ma, Y.-L.; Zhou, H.; Rissanen, K.; Jiang, W. A supramolecular system that strictly follows the binding mechanism of conformational selection. *Nature Communications* **2020**, *11*, 2740.
- (27) Rovó, P.; Smith, C. A.; Gauto, D.; de Groot, B. L.; Schanda, P.; Linser, R. Mechanistic Insights into Microsecond Time-Scale Motion of Solid Proteins Using Complementary  $^{15}\text{N}$  and  $^1\text{H}$  Relaxation Dispersion Techniques. *J. Am. Chem. Soc.* **2019**, *141*, 858–869.
- (28) Chandler, D. *Introduction to Modern Statistical Mechanics*; Oxford University Press, 1987.

- (29) Abraham, M. J.; Murtola, T.; Schulz, R.; Pll, S.; Smith, J. C.; Hess, B.; Lindahl, E. GRO-MACS: High performance molecular simulations through multi-level parallelism from laptops to supercomputers. *SoftwareX* **2015**, *1-2*, 19–25.
- (30) Song, L. F.; Lee, T.-S.; Zhu, C.; York, D. M.; Merz, K. M. Using AMBER18 for Relative Free Energy Calculations. *J. Chem. Inf. Model.* **2019**, *59*, 3128–3135, PMID: 31244091.
- (31) Jiang, W.; Chipot, C.; Roux, B. Computing Relative Binding Affinity of Ligands to Receptor: An Effective Hybrid Single-Dual-Topology Free-Energy Perturbation Approach in NAMD. *J. Chem. Inf. Model.* **2019**, *59*, 3794–3802, PMID: 31411473.
- (32) Bhati, A. P.; Wan, S.; Hu, Y.; Sherborne, B.; Coveney, P. V. Uncertainty Quantification in Alchemical Free Energy Methods. *J. Chem. Theory Comput.* **2018**, *14*, 2867–2880.
- (33) Procacci, P. Does Hamiltonian Replica Exchange via Lambda-Hopping Enhance the Sampling in Alchemical Free Energy Calculations? *Molecules* **2022**, *27*.
- (34) Yildirim, A.; Wassenaar, T. A.; van der Spoel, D. Statistical efficiency of methods for computing free energy of hydration. *J. Chem. Phys.* **2018**, *149*, 144111.
- (35) Manzoni, F.; Ryde, U. Assessing the stability of free-energy perturbation calculations by performing variations in the method. *J. Comput.-Aided Mol. Des.* **2018**, *32*, 529–536.
- (36) Coveney, P. V.; Wan, S. On the calculation of equilibrium thermodynamic properties from molecular dynamics. *Phys. Chem. Chem. Phys.* **2016**, *18*, 30236–30240.
- (37) Hahn, D. F.; König, G.; Hunenberger, P. H. Overcoming Orthogonal Barriers in Alchemical Free Energy Calculations: On the Relative Merits of  $\lambda$ -Variations,  $\lambda$ -Extrapolations, and Biasing. *J. Chem. Theory Comput.* **2020**, *16*, 1630–1645,  
Thorough study on the merits of various enhanced sampling techniques in FEP application, highlighting the importance of the biasing approaches (e.g. REST ).
- (38) Procacci, P. Methodological uncertainties in drug-receptor binding free energy predictions based on classical molecular dynamics. *Current Opinion in Structural Biology* **2021**, *67*, 127–134.

- (39) Fukunishi, H.; Watanabe, O.; Takada, S. On the Hamiltonian replica exchange method for efficient sampling of biomolecular systems: Application to protein structure prediction. *J. Chem. Phys.* **2002**, *116*, 9058–9067.
- (40) Liu, P.; Kim, B.; Friesner, R. A.; Berne, B. J. Replica exchange with solute tempering: A method for sampling biological systems in explicit water. *Proc. Acad. Sci.* **2005**, *102*, 13749–13754.
- (41) Sindhikara, D. J.; Emerson, D. J.; Roitberg, A. E. Exchange Often and Properly in Replica Exchange Molecular Dynamics. *J. Chem. Theory Comput.* **2010**, *6*, 2804–2808, PMID: 26616081.
- (42) Nadler, W.; Meinke, J. H.; Hansmann, U. H. E. Folding proteins by first-passage-times-optimized replica exchange. *Phys. Rev. E* **2008**, *78*, 061905.
- (43) Nadler, W.; Hansmann, U. H. E. Optimized Explicit-Solvent Replica Exchange Molecular Dynamics from Scratch. *The Journal of Physical Chemistry B* **2008**, *112*, 10386–10387, PMID: 18671362.
- (44) Hewings, D. S.; Wang, M.; Philpott, M.; Fedorov, O.; Uttarkar, S.; Filippakopoulos, P.; Picaud, S.; Vuppusetty, C.; Marsden, B.; Knapp, S.; Conway, S. J.; Heightman, T. D. 3,5-Dimethylisoxazoles Act As Acetyl-lysine-mimetic Bromodomain Ligands. *J. Med. Chem.* **2011**, *54*, 6761–6770, PMID: 21851057.
- (45) Jakalian, A.; Jack, D. B.; Bayly, C. I. Fast, efficient generation of high-quality atomic charges. AM1-BCC model: II. Parameterization and validation. *J. Comput. Chem.* **2002**, *23*, 1623–1641.
- (46) Procacci, P. PrimaDORAC: A Free Web Interface for the Assignment of Partial Charges, Chemical Topology, and Bonded Parameters in Organic or Drug Molecules. *J. Chem. Inf. Model.* **2017**, *57*, 1240–1245.
- (47) Lindorff-Larsen, K.; Piana, S.; Palmo, K.; Maragakis, P.; Klepeis, J. L.; Dror, R. O.;

- Shaw, D. E. Improved side-chain torsion potentials for the Amber ff99SB protein force field. *Proteins* **2010**, *78*, 1950–1958.
- (48) Nosé, S. A unified formulation of the constant temperature molecular dynamics methods. *J. Chem. Phys.* **1984**, *81*, 511–519.
- (49) Jorgensen, W. L.; Chandrasekhar, J.; Madura, J.; Impey, R.; Klein, M. Comparison of simple potential functions for simulating liquid water. *J. Chem. Phys.* **1983**, *79*, 926–935.
- (50) Marchi, M.; Procacci, P. Coordinates scaling and multiple time step algorithms for simulation of solvated proteins in the NPT ensemble. *J. Chem. Phys.* **1998**, *109*, 5194–5202.
- (51) Essmann, U.; Perera, L.; Berkowitz, M. L.; Darden, T.; Lee, H.; Pedersen, L. G. A smooth particle mesh Ewald method. *J. Chem. Phys.* **1995**, *103*, 8577–8593.
- (52) Procacci, P. Hybrid MPI/OpenMP Implementation of the ORAC Molecular Dynamics Program for Generalized Ensemble and Fast Switching Alchemical Simulations. *J. Chem. Inf. Model.* **2016**, *56*, 1117–1121.
- (53) Caves, L. S. D.; Evanseck, J. D.; Karplus, M. Locally accessible conformations of proteins: Multiple molecular dynamics simulations of crambin. *Protein Science* **1998**, *7*, 649–666.
- (54) Gapsys, V.; Yildirim, A.; Aldeghi, M.; Khalak, Y.; van der Spoel, D.; de Groot, B. L. Accurate absolute free energies for ligand-protein binding based on non-equilibrium approaches. *Comm. Chem.* **2021**, *4*, 61.
- (55) Rusina, P.; Gandalipov, E.; Abdusheva, Y.; Panova, M.; Burdenkova, A.; Chaliy, V.; Brachs, M.; Stroganov, O.; Guzeeva, K.; Svitanko, I.; Shtil, A.; Novikov, F. Imidazole-4-N-acetamide Derivatives as a Novel Scaffold for Selective Targeting of Cyclin Dependent Kinases. *Cancers* **2023**, *15*.
- (56) Jarzynski, C. Nonequilibrium equality for Free energy differences. *Phys. Rev. Lett.* **1997**, *78*, 2690–2693.

- (57) Crooks, G. E. Nonequilibrium measurements of free energy differences for microscopically reversible Markovian systems. *J. Stat. Phys.* **1998**, *90*, 1481–1487.

For Table of Contents Only